Relative errors of derived multi-wavelength intensive aerosol optical properties using CAPS PM$_{SSA}$, Nephelometer, and TAP measurements

5   Patrick Weber[1], Andreas. Petzold[1], Oliver F. Bischof[1,2], Benedikt Fischer[1], Marcel Berg[1], Andrew Freedman[3], Timothy B. Onasch[3], Ulrich Bundke[1]

[1]Forschungszentrum Jülich GmbH, Institute of Energy and Climate Research 8 – Troposphere (IEK-8), Jülich, Germany

[2]TSI GmbH, Particle Instruments, Aachen, Germany

10 [3]Aerodyne Research Inc., Billerica, MA 01821, USA

Correspondence to: Ulrich Bundke (u.bundke@fz-juelich.de)

Abstract. Aerosol intensive optical properties, including Ångström exponents for aerosol light extinction (EAE), scattering (SAE), and absorption (AAE), and the single-scattering albedo (SSA), are indicators for aerosol size, chemical composition, radiative behaviour, and particle sources. Derivation of these parameters requires the

15 measurement of aerosol optical properties at multiple wavelengths, which usually involves the use of several instruments. Our study aims to quantify the uncertainties in the determination of these intensive properties using an optical closure approach. In our laboratory closure study, we measured the full set of optical properties for a range of light-absorbing particles with different properties externally mixed with ammonium sulphate to generate aerosols with controlled SSA values. The investigated absorbing particle types were: fresh combustion soot emitted by an inverted

20 flame soot generator (SOOT, fractal agglomerates), Aquadag (AQ, compact aggregates), Cabot industrial soot (BC, compact agglomerates), and an acrylic paint (Magic Black, shape unknown). The instruments used in this study were two Cavity Attenuated Phase Shift Single Scattering Albedo monitors (CAPS PM$_{SSA}$, λ = 450, 630 nm) for measuring light extinction and scattering coefficients, one Integrating Nephelometer (λ = 450, 550, 700 nm) for light scattering coefficients, and one Tricolour Absorption Photometer (TAP, λ = 467, 528, 652 nm) for filter-based light absorption

25 coefficients.

One key finding is that the coefficients of light absorption, scattering, and extinction derived from combing the measurements of two independent instruments agree with measurements from single instruments; the slopes of regression lines are equal within reported uncertainties (i.e., closure is observed). Despite closure for measured

30 absorption coefficients, we caution that the estimated uncertainties for absorption coefficients, propagated for the Differential Method (DM: absorption = extinction minus scattering), can exceed 100% for atmospheric relevant SSA values (>0.9). This increasing estimated uncertainty with increasing SSA yields AAE values that may be too uncertain for measurements in the range of atmospheric aerosol loadings. We recommend using DM for measuring AAE values when the SSA < 0.9. EAE and SAE derived values achieved closure during this study within stated uncertainties for

35 extinction coefficients greater than 15 Mm^{-1}. SSA values for 450 nm and 630 nm wavelengths internally agreed with each other within 10% uncertainty for all instrument combinations and sampled aerosol types which fulfils the defined

goals for measurement uncertainty of 10% proposed by Laj et al., 2020 for GCOS (Global Climate Observing System) applications.

40 **1. Introduction**

The precise determination of aerosol optical properties is crucial for the provision of reliable input data for chemistry transport models, climate models, and radiative forcing calculations (Myhre et al., 2013). This applies, in particular, to light-absorbing particles like black carbon (Petzold et al., 2013), which are produced by incomplete combustion

45 processes and absorb visible light very efficiently. Aerosol light absorbing properties are also relevant for source appointment studies and the determination of anthropogenic influences on atmospheric aerosols (Sandradewi et al., 2008). There are two common methods to generate aerosol light absorption values for long-term and short-term monitoring, each with its own disadvantages. One method is a filter-based technique, which operates by deriving light absorbing values from the attenuation of light through particle-loaded filters (Rosen et al., 1978). A disadvantage of

50 all filter-based methods is linked to artifacts like multiple scattering inside the filter matrix, shadowing of light-absorbing particles in highly loaded filters, and humidity effects on the filter substrate (Lack, 2008; Moosmüller et al., 2009). Widely deployed filter-based light absorption instruments include the Particle Soot Absorption Photometer (PSAP: Bond et al., 1999), the Tri-colour Absorption Photometer (TAP), the Continuous Light Absorption Photometer (CLAP; Ogren et al., 2017), the Aethalometer (Hansen et al., 1984), and the Multi-Angle Absorption Photometer

55 (MAAP) (Petzold et al., 2005). The PSAP, TAP, CLAP, and Aethalometer share their measurement principle, utilize a reference spot technique, and require complex correction algorithms (Coen et al., 2010; Virkkulaet al., 2010; Virkkula et al., 2005). The MAAP utilizes a different approach, a two-stream radiative transport model, made possible by its measurement of both direct transmission and back scatter from the particle loaded filter substrate. Another method for deriving aerosol light absorption is the differential method, based on the subtraction of light scattering

60 from extinction. This method is commonly conducted by comparing measurements from two separate instruments which results in large precision errors particularly for low light absorption and/or high single scattering albedo (SSA) values. In laboratory studies, however, the differential method is widely used as a reference technique because the applied light scattering and extinction instruments make measurements on freely floating particles (i.e., no filter-based artifacts) and are well characterised (Bond et al., 1999; Schnaiter et al., 2005; Sheridan et al., 2005). A significant

65 improvement of aerosol measurement capacities is achieved by the recently developed Cavity Attenuated Phase Shift particle monitor for single scattering albedo (CAPS PM_{SSA}) (Onasch et al., 2015), which is able to measure light extinction and scattering simultaneously and is the focus of recent studies (Perim de Faria et al., 2021; Modini et al., 2021).

70 Intensive aerosol parameters like the Single Scattering Albedo (SSA) or Ångström exponents are often not directly measured, but calculated from multiple instrument datasets, which could lead to an increase in errors and uncertainties. The importance of measuring reliable intensive parameters is undisputable, especially when their use is required for an experiment or sensitive climate related modelling. The Ångström exponents are widely used to adjust extensive

parameters to a desired wavelength (Ångström, 1929)for instrument comparisons (Foster et al. 2019), for aerosol characterisation (Russell et al., 2010) like the refraction index determination of mineral dust (Petzold et al., 2009) or black carbon (Kim et al., 2015), or for source identification of mineral dust (Formenti et al., 2011). Ångström exponents vary with particle size, shape, and chemical composition, though the relative importance of these factors differ for each optical property. The scattering Ångström exponent (SAE) is most sensitive to particle size and, therefore, used as an indication of the size distribution of measured aerosols. A SAE value of 4 indicates either gaseous Rayleigh scattering or nanometre-sized particles, whereas a value of 0 indicates coarse particles (Kokhanovsky, 2008). The absorption Ångström exponents (AAE) is sensitive to the chemical composition and size of the aerosol particles. A value of 1 indicates an aerosol which absorbs light strongly across the entire visible spectral range and is composed of nanometre-sized spherules (Berry and Percival, 1986). This behaviour is characteristic for fresh soot or black carbon fractal agglomerates (Kirchstetter and Thatcher, 2012; Xu et al., 2015). AAE values higher than unity indicate the presence of brown carbon (Kim et al., 2015) or mineral dust (Formenti et al., 2011), both of which are characterised by a stronger absorption in the blue and ultraviolet compared to the red spectral range. AAE values > 1 may also occur for coated light absorbing particles (e.g., coated soot) or larger, more compact light absorbing particles (Lack and Cappa, 2010). The extinction Ångström exponent (EAE) is often used for aerosol classification by remote sensing methods such as Lidar and depends on particle size and chemical composition (Kaskaoutis et al., 2007; Veselovskii et al., 2016). Combining these Ångström exponents in cluster plots is a reliable method for classifying aerosol sources (Russell, 2010). The SSA of an aerosol is the key parameter for its direct and semi direct impact on climate (Penner, 2001). The SSA describes the ratio of scattering to total extinction of a measured aerosol. An SSA value of 1 indicates that light extinction occurs exclusively due to light scattering. In contrast, SSA values < 1 indicate an aerosol with a significant fraction of light-absorbing components, which may cause heating of the atmosphere. The intensive parameters are commonly available only through multiple-instrument approaches at different wavelengths, which calls for a detailed analysis of their measurement uncertainties. Our study contributes to this topic with a detailed optical closure study, in which we deploy standard and advanced instrumentation for measuring aerosol optical properties and sample mixtures of light absorbing and scattering aerosol to assess method uncertainties and precision errors.

2. Experimental Approach

2.1 Experimental Design

A schematic of the experimental setup is shown in Figure 1. Briefly, aerosol flows, generated using two nebulizers or an inverted flame generator, are dehumidified (generally to below 7%) using diffusion driers filled with silica gel and sent to a mixing chamber to ensure homogeneous mixing, prior to being sampled using a suite of optical instruments. In order to avoid particle losses caused by electrostatic forces, all tubing and chambers are constructed of either stainless steel or conductive silicone tubing. The individual optical instruments are connected using an iso-axial orientated and isokinetic operated nozzle located in the centreline of the supply line. As shown in Figure 1, aerosol production was controlled by multiple Mass Flow Controllers (MFC, Bronkhorst High-Tech B.V., Ruurlo,

Netherlands). A Labview based program controlled the complete measurement system and centrally recorded all data from the individual instruments. Pressures in the aerosol delivery lines were maintained at that of the ambient atmosphere at all times. Aerosol flow rates to the individual instruments were provided at their specified levels (0.6 - 3.0 lpm) except for that of the TSI nephelometer. Given the limitations of the aerosol supply system, the flow to the nephelometer was reduced from 20 lpm to 2.2 lpm, causing the physical response time of that instrument to be increased to ten minutes. Complete details of the generation of aerosols are provided in the following section.
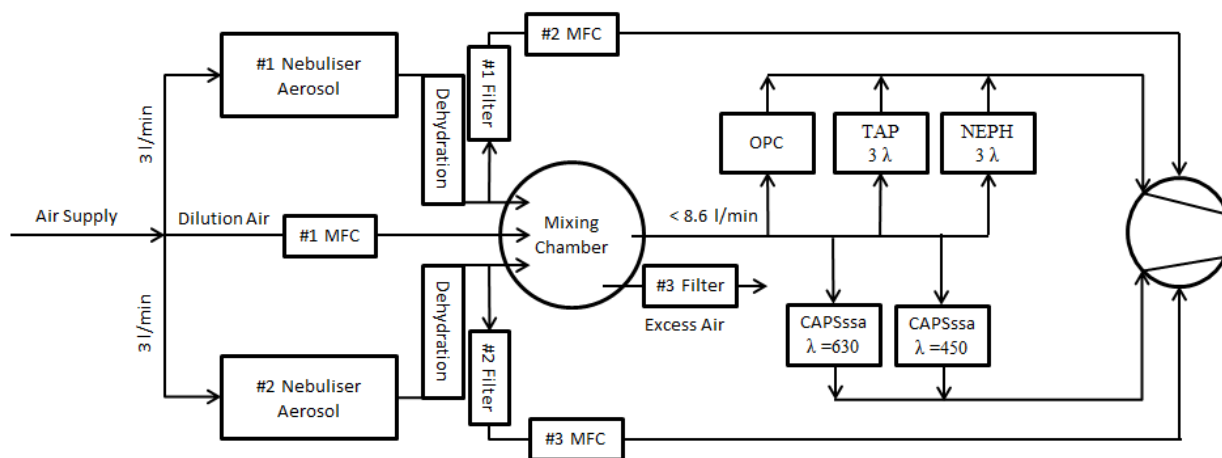
Figure 1. Experimental setup for the measurements. Flame soot measurements were done with a combustion flame source replacing #2 Nebuliser.

The generated aerosol size distributions were characterized and monitored with either a Scanning Mobility Particle Sizer (SMPS) composed of the combination of a Differential Mobility Analyzer (DMA 5.400, Grimm Aerosol Technik GmbH Co & KG Germany) and Condensation Particle Counter (CPC 5.411, Grimm Aerosol Technik) system in a sequential mode of operation or a Grimm optical particle size spectrometer (SKY-OPC, model 1.129, Grimm Aerosol GmbH & Co. KG, Ainring, Germany).

2.2 Optical Instruments and Uncertainties

The suite of optical instruments used in this study included the following instruments. The particle scattering coefficient, σ_{sp}, was measured with an integrating multi wavelength nephelometer (NEPH, Model 3563, TSI Inc., Shoreview, MN, USA; Bodhaine et al., 1991) and with the scattering channel of the CAPS PM$_{SSA}$ monitor (CAPS PM$_{SSA}$, Aerodyne Research Inc., Billerica, MA, USA; Onasch et al. (2015), which is derived from a measurement of the total extinction and single scattering albedo. For the particle light absorption coefficient, σ_{ap}, we used the Tricolor Absorption Photometer (TAP (Brechtel Inc., Hayward, CA, USA), which is based on the well-known Particle Soot Absorption Photometer (PSAP, ARM Research) and the Continuous Light Absorption Photometer (CLAP) developed by NOAA (Ogren et al., 2017). The particle light extinction coefficient, σ_{ep}, was directly measured with the phase shift channel of the CAPS PM$_{SSA}$ monitor.

The light extinction channel of the CAPS instrument has an uncertainty of 5% and a precision of 2% and a scattering uncertainty of 8% and 2% precision, respectively (Onasch et al., 2015). The TAP has an uncertainty of around 8%, with a precision of 4% ((Müller et al., 2014; Ogren et al., 2017), while the NEPH has an uncertainty of less than 10% and a precision of about 3% (Anderson and Ogren, 1998 Massoli et al., 2009). These literature-derived uncertainty estimates for measurement accuracy will be used in this study for instrument closure, either directly or via error propagation. Individual point averages will be shown with corresponding precision variances.

2.3 Aerosol Generation

Table 1 provides a complete list of all aerosol types used in the study. Solutions of known concentrations of Aquadag (AQ, Aqueous Deflocculated Acheson Graphite; Acheson Industries, Inc., Port Huron, MI, USA), Cabot Black (BC) and Magic Black (MB), an acrylic based paint, were prepared on a daily basis by ultra-sonication before nebulization in a Constant Output Atomizer (Model 3076, TSI Inc.). The count median diameter (CMD) and geometric standard deviation (GSD) of the ammonium sulphate nebulized by the constant output atomizer depends on the concentration of the salt solution and the flow through the atomizer. Use of constant flow rates and particle concentrations produced constant size distributions (Liu et al. 1975). The inverted flame soot generator (Argonaut Scientific Corporation, Edmonton, AB, Canada) was operated with a pre-determined propane to oxidation air ratio of 7.5 litre per minute air to 0.0625 litre per minute propane so that the flame produced a stable and low organic carbon soot. It has previously been shown that at least 30 min were necessary for the Argonaut flame to reach stable aerosol concentrations (Bischof et al., 2019; Kazemimanesh et al., 2018).

Initially, pure aerosol types were generated independently and measured to quantify their size distributions and optical properties. The main part of the study was focused on making external mixtures of ammonium sulphate and each of the absorbing particle types, separately. These mixtures were controlled to provide a stable aerosol with varying intensive optical properties.

Table 1. Overview of aerosol types used.

Substance	Aerosol type	Acronym	Shape
Ammonium Sulphate	salt	AS	spheroidal
Aquadag	colloidal graphite	AQ	compact aggregates
Cabot Black (Regal 400R)	powder	BC	compact agglomerates
Flame Soot	combustion aerosol	Soot	fractal agglomerates
Magic Black (Acrylic paint)	organic pigments	MB	unknown

2.4 Data Treatment

2.4.1 Instrument Corrections and Calibrations

The CAPS PM$_{SSA}$ instrument extinction channel was calibrated using polystyrene latex beads (PSL) particles as a reference standard and Mie theory using a BHMIE Python code derived from Bohren & Hoffman (1983). Additionally,

the 450 nm wavelength CAPS PM_{SSA} calibration was validated using measurements of CO_2 Rayleigh scattering . The scattering channel of the CAPS PM_{SSA} was internally adjusted to the extinction channel using ammonium sulphate as a light-scattering aerosol, assuming a single scattering albedo of 1.0. A truncation error correction was not necessary regarding the size of the aerosols used (Onasch et al., 2015), since all the aerosols used had median diameter smaller than 200 nm. The CAPS PM_{SSA} monitor, which is subject to baseline drift as the system heats up, stabilized after 30 min of operation (Faria et al., 2019).

The NEPH was calibrated using CO_2 (Anderson and Ogren, 1998; Modini et al., 2021). Truncation corrections were made using the approaches developed by Anderson and Ogren (1998) for purely scattering aerosols and by Massoli et al. (2009) for aerosol mixtures containing light absorbing particles. The truncation corrections applied were always equal to or less than 5%. Because of the reduced air flow, the NEPH needed at least 15 minutes to reach a stable plateau after changing aerosol generation settings.

A new filter spot for the TAP was selected for each measurement in order to minimize measurements uncertainties due to particle loaded filters. The first correction regarding truncation is done by the included Software. The software has the capability to choose the Ogren correction scheme based on the filter type used (Quartz Fibre, BT-TAP-FIL100, ENVILYSE). Further corrections were made according to Virkkula, (2010).

Table 2. List of applied correction algorithms to optical instruments.

Instrument	Manufacturer	Properties	λ (nm)	Reference
CAPS PM_{SSA}	Aerodyne Research Inc.	σ_{ep}; σ_{sp}	450; 630	Onasch et al. (2015)
NEPH	TSI Inc.	σ_{sp}	450; 550;700	Anderson and Ogren (1998); Massoli et al. (2009)
TAP	Brechtel Inc.	σ_{ap}	467; 530; 660	Virkkula (2010); Virkkula (2005)

2.4.2 Aerosol Optical Properties derived from primary measurements

The extensive parameters for aerosol light interactions are extinction, scattering and absorption. When two of them are known, the missing one can be calculated with the help of this equation:

$$\sigma_{ep} = \sigma_{sp} + \sigma_{ap} \hspace{4cm} \text{Eq. (1)}$$

where σ_{ep} is the extinction coefficient, σ_{sp} the light scattering coefficient and σ_{ap} the coefficient for light absorption by particles. The unit of all these parameters is Mm^{-1} ("inverse Mega meters"; $1\ Mm^{-1} = 10^{-6}\ m^{-1}$). When solving equation 1 for σ_{ap}, it is possible to derive the absorption coefficient by combining CAPS PM_{SSA} extinction measurements with either CAPS PM_{SSA} or NEPH scattering measurements [σ_{ap}(CAPS, CAPS) or σ_{ap}(CAPS, NEPH)] for comparison. In the following, this will be called the Differential Method (DM).

To calculate the Single Scattering Albedo (SSA), the particle light scattering must be divided by the particle light extinction:

$$(\lambda) = \frac{\sigma_{sp}}{\sigma_{ep}} \qquad \text{Eq. (2)}$$

The Ångström exponents (AE) are calculated from:

$$xAE = -\frac{\log\left(\frac{\sigma_{xp}(\lambda 1)}{\sigma_{xp}(\lambda 2)}\right)}{\log(\lambda 1/\lambda 2)} \qquad \text{Eq. (3)}$$

By solving Eq. 3 for $\sigma_p(\lambda 1)$ and assuming a valid Ångström exponent the resulting equation (3a) is used for wavelength adjustments

$$\sigma_{xp}(\lambda 1) = \sigma_{xp}(\lambda 2) \cdot \left(\frac{\lambda 1}{\lambda 2}\right)^{-AE} \qquad \text{Eq. (3a)}$$

For the particle coefficient σ_{xp}, the corresponding σ_{sp}, σ_{ep}, or σ_{ap} could be put into calculations (Eq. 3) to obtain the absorption Ångström exponent (AAE), extinction Ångström exponent (EAE) and scattering Ångström exponent (SAE), accordingly.

2.4.3 Error propagation

Error propagation are determined by Gaussian error propagation:

$$SSA(\lambda, \sigma_{sp}, \sigma_{ep}) = \frac{\sigma_{sp}}{\sigma_{ep}} \xrightarrow{yields} \Delta SSA(\lambda, \sigma_{sp}, \sigma_{ep}) = \sqrt{\left(\frac{1}{\sigma_{ep}} \cdot \Delta\sigma_{sp}\right)^2 + \left(\frac{\sigma_{sp}}{\sigma_{ep}^2}\Delta\sigma_{ep}\right)^2} \qquad \text{Eq. (4)}$$

$$SSA(\lambda, \sigma_{sp}, \sigma_{ap}) = \frac{\sigma_{sp}}{\sigma_{ap}+\sigma_{sp}} \xrightarrow{yields} \Delta SSA(\lambda, \sigma_{sp}\sigma_{ap}) = \sqrt{\left(\frac{\sigma_{sp}}{(\sigma_{ap}+\sigma_{sp})^2} \cdot \Delta\sigma_{sp}\right)^2 + \left(\frac{\sigma_{ap}}{(\sigma_{ap}+\sigma_{sp})^2} \cdot \Delta\sigma_{ap}\right)^2} \qquad \text{Eq. (5)}$$

$$AE = -\frac{\log\left(\frac{\sigma_{xp}(\lambda 1)}{\sigma_{xp}(\lambda 2)}\right)}{\log(\lambda 1/\lambda 2)} \xrightarrow{yields} \Delta AE = \sqrt{\left(\frac{-1}{\log(\lambda 1/\lambda 2)\cdot\sigma_p(\lambda 1)} \cdot \Delta\sigma_{xp}(\lambda 1)\right)^2 + \left(\frac{1}{\log(\lambda 1/\lambda 2)\cdot\sigma_{xp}(\lambda 2)} \cdot \Delta\sigma_p(\lambda 2)\right)^2} \qquad \text{Eq (6)}$$

where $\sigma_{xp} = \{\sigma_{ep}, \sigma_{sp}, \sigma_{ap}\}$

Those equations could be expanded, if the instruments where not calibrated properly, as Sherman (2015) proposed, but are in accordance with the BIPM (Bureau International des Poids et Mesures)

2.4.4 Data Averaging

For each experiment run, a different aerosol mixture was generated with different optical properties and allowed to reach steady state, including waiting ~15 minutes due to the slow time response of the low flow NEPH. At steady state conditions, we measured size and optical properties fluctuating <2% over time with the OPC, CAPS PM$_{SSA}$, and NEPH. All instruments recorded data at a 1 second rate. Reported data points are given as averages of 100 seconds of stable aerosol production. This value was chosen to obtain a minimum in data precision and detection limits as determined from Allan Standard Deviation plots by Massoli et al. (2010) for the CAPS extinction measurements and Ogren et al. (2017) for filter-based absorption measurements. Averaging for longer periods would only increase variances due to transmission (TAP) and baseline drift (CAPS).

3. Measurements

3.1 Pure aerosol types

The measured size parameters and calculated intensive parameters of the pure aerosol types are summarized in Table
3. The errors reported in Table 3 are calculated from error propagation. The size distributions of the different aerosol
types were measured with a Grimm SMPS and are shown in Figure 2 normalized to 1000 particles per cubic
centimetre. The Ångström exponents for the pure substances fall within typical ranges for these types of aerosols and
size distributions reported in literature. For example, the SAE decreases from a value of 3.22 for 40 nm AS particles
which is close to the SAE value of 4 for air molecules with increasing particle diameter. Thus, the SAE drops to 0.76
for 130 nm compact AQ particles but increases to 0.99 for 140 nm fractal agglomerate Soot. The shape of AQ is
assumed to be more compact than the soot agglomerates, such that their scattering and electrical mobility behaviours
are dependent mainly upon their physical diameters. In contrast, the scattering behaviour of the fractal soot
agglomerates is due mainly to the distribution of primary particles, whereas their electrical mobility diameter is more
dependent upon the major axis of the agglomerate. As expected by Eq. 3a, the SSA increases with decreasing
wavelength (Bohren and Huffman, 1983). The AAE for fractal combustion soot is close to 1 as reported by Török
(2018) for the mini-CAST soot generator.
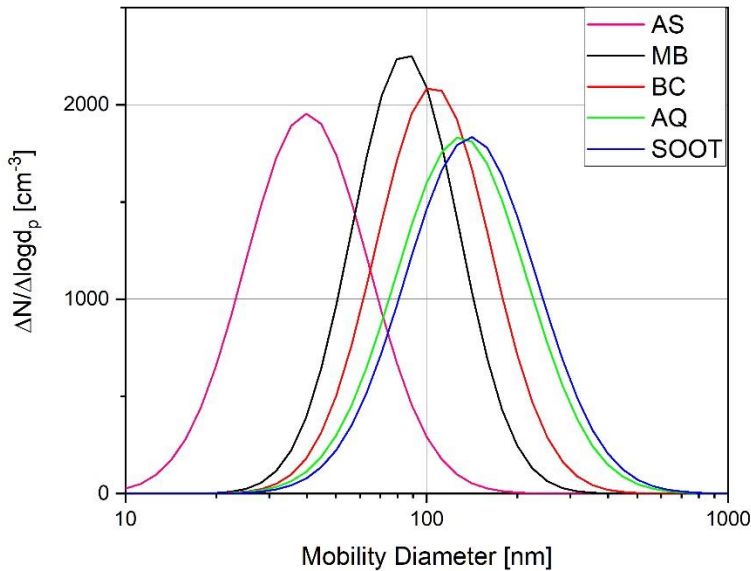
Figure 2. Measured size distributions by SMPS for the pure aerosol types used, normalised to an assumed total
concentration.

Table 3. Overview of the measured intensive optical properties of the pure aerosol types.

	AS	MB	BC	AQ	Soot

Count Median Diam.	40 nm	85 nm	105 nm	130 nm	140 nm
Geometric Standard Deviation	1.60	1.50	1.55	1.65	1.65
SSA 630 (NEPH, CAPS)	1.0	0.85 ± 0.02	0.26 ± 0.03	0.37 ± 0.03	0.20 ± 0.02
SSA 450 (NEPH, CAPS)	1.0	0.92 ± 0.07	0.32 ± 0.04	0.44 ± 0.02	0.26 ± 0.08
SAE (630/450) (NEPH)	3.22 ± 0.09	2.16 ± 0.37	1.71 ± 0.13	0.76 ± 0.06	0.99 ± 0.08
AAE (630/450) (TAP)	-	1.34 ± 0.12	1.16 ± 0.03	0.44 ± 0.02	1.08 ± 0.02
EAE (630/450) (CAPS)	3.21 ± 0.08	2.03 ± 0.38	1.43 ± 0.65	0.52 ± 0.10	1.10 ± 0.10

3.2 Extensive Parameters of Aerosol Mixtures

255 First, the extensive parameters must be validated for all instrument combinations to ensure the reliability of the intensive parameters derived from them. We have chosen to use external mixtures of AS and AQ particles for these studies as they are both readily atomized, generating highly stable aerosols for the necessary time periods for averaging. We note that AQ absorbing aerosols are commonly used as a reference material for instrument comparisons (Foster et al., 2019). The results for mixtures of AS with the other absorbing aerosol types are included in Tables 6-9.

260

The two CAPS PM_{SSA} monitors (450 nm and 630 nm wavelengths) measured the extinction coefficient of particles directly with a small precision error of around 2% (Modini et al., 2021). In Figure 3, we show scatter plots of these direct extinction coefficient measurements (X-axis) in comparison to the absorption coefficient measured using TAP and the scattering coefficient measured using NEPH combined using Equation (Eq. 1) in the form:

265 $\sigma_{ep}(NEPH, TAP) = \sigma_{ap}(TAP) + \sigma_{sp}(NEPH)$ (y-axis) for wavelengths of 450 nm (right panel) and 630 nm (left panel).
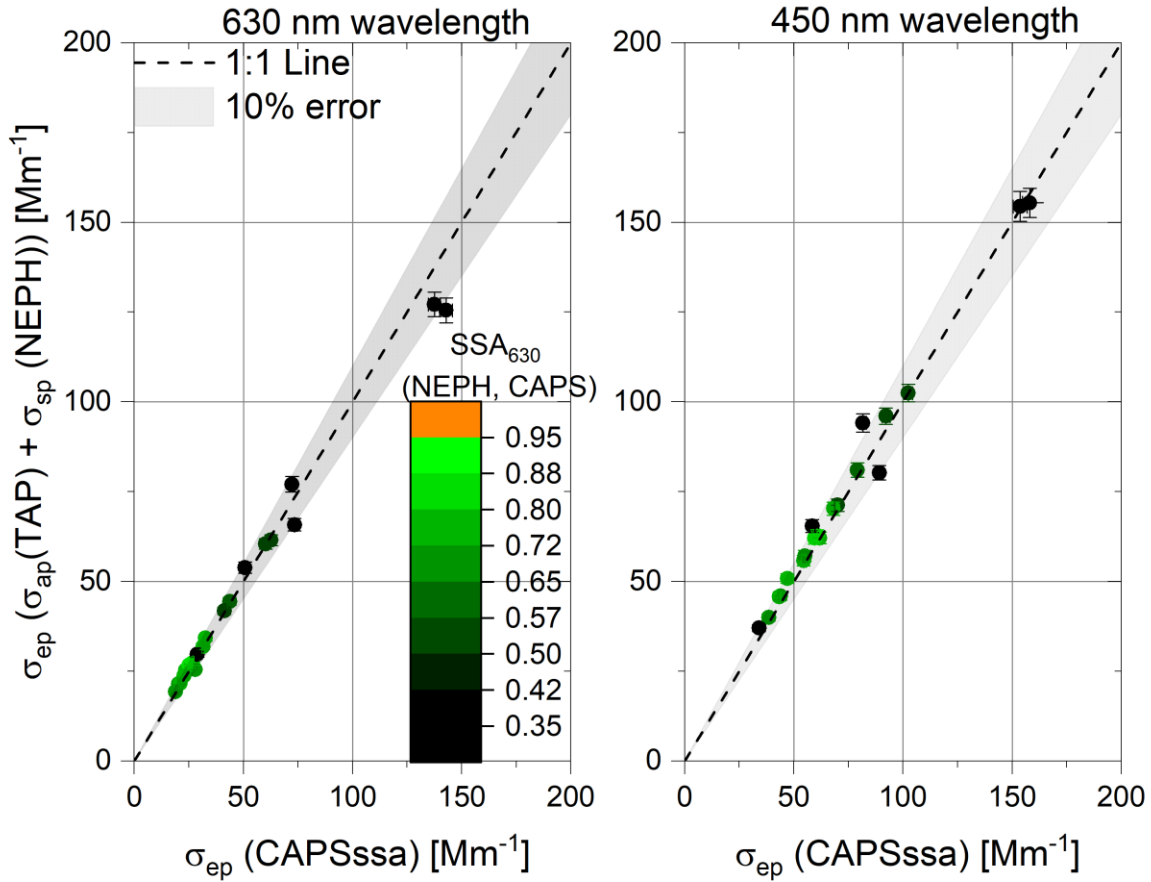
Figure 3. Scatter plots of the extinction coefficients for different AQ-AS external mixtures at 630 nm (left) and 450 nm wavelengths (right). The y-axes show the extinction coefficients derived by combining TAP absorption and NEPH scattering coefficients versus the CAPS PM_{SSA} monitor direct extinction coefficient measurements. The colour code represents the SSA of the analysed mixed aerosol measured at 630 nm wavelength. In addition, an error band of ±10% was added to the 1:1 line.

Here, the measured 630 nm SSA colour code serves as a proxy for the mixing ratio of the external mixtures of nebulized AQ and AS particles. The measured 630 nm and 450 nm extinction coefficients align with the 1:1 line within 10% across a broad range of extinction values as well as SSA values, ranging from 0.3 to close to 1. The 10% was chosen to show the fulfilment of the requirements of Laj, 2020 for aerosol properties. This shows that the instruments are not sensitive to the SSA of the particle type used at either wavelength of interest.

The measured scattering coefficients at 450 and 630 nm wavelengths are compared using scatterplots for the different techniques in Figure 4. Here, we use the NEPH and the integrating sphere channel of the CAPS PM_{SSA} instrument capable of measuring the scattering coefficient directly. In addition, we calculated the scattering coefficients using a Differential Method (DM), solving Eq.(1) for the scattering coefficient by subtracting the absorption coefficient

measured by the TAP from the extinction coefficient measured by CAPS PM$_{SSA}$, The NEPH is used as reference
because it has well proven correction functions for light absorption particles, as described in Section 2.4.1.
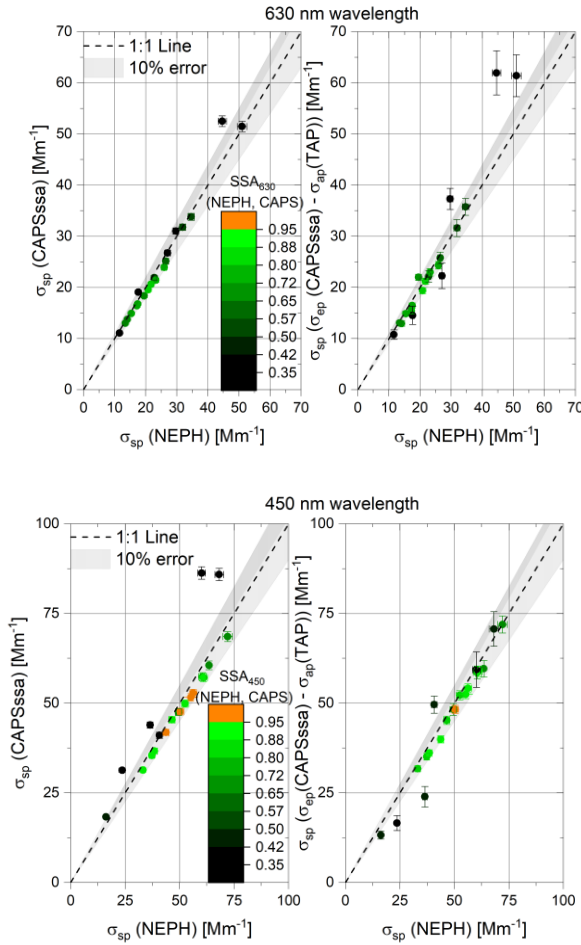
Figure 4. Comparisons of measured light scattering coefficients at 450 nm and 630 nm wavelengths for mixtures of
AQ and AS aerosols. The y-axes show the CAPS PM$_{SSA}$ (integrating sphere) or the Differential Method (CAPS
extinction minus TAP absorption) scattering versus NEPH scattering measurements at 450 nm and 630 nm
wavelengths. The colour code represents the SSA value of the measured aerosol mixture. An error band of ±10% was
applied to the 1:1 line. Error bars shown represent instrument precisions (1 σ).

The measured scattering coefficients at both 450 nm and 630 nm wavelengths agree within 10% for the majority of
measurements. There is no apparent dependence of measured scattering coefficients with scattering coefficient
magnitude (over the range measured) nor with aerosol SSA, an indicator of the external mixing ratio. Several outliers
are visible, particularly for points with SSA values ~ 0.35, indicating nearly pure AQ aerosols. For the scattering
coefficients derived using the Differential Method (CAPS extinction minus TAP absorption), some of the scatter may
be due to the larger uncertainties associated with the filter-based absorption measurements, as discussed in the Reno
Study (Sheridan, 2005). The outliers in the CAPS vs NEPH plots, especially at 450 nm wavelength, are currently
unexplained and are likely due to apparent stability issues for these points.

Particle light absorption coefficient measurements are the most complicated, as none of our optical instrument techniques directly measure absorption. We have two methods for measuring absorption coefficients: (1) Differential Method following Eq.(1), using either $\sigma_{ap}(CAPS,NEPH) = \sigma_{ep}(CAPS) - \sigma_{sp}(NEPH)$ or $\sigma_{ap}(CAPS,CAPS) = \sigma_{ep}(CAPS) - \sigma_{sp}(CAPS)$; and (2) filter-based TAP measurements. As the filter-based method requires the application of multiple, empirical correction schemes, we have chosen $\sigma_{ap}(CAPS,NEPH)$ as the reference for the comparison of the $\sigma_{ap}(TAP)$ and $\sigma_{ap}(CAPS,CAPS)$ values.
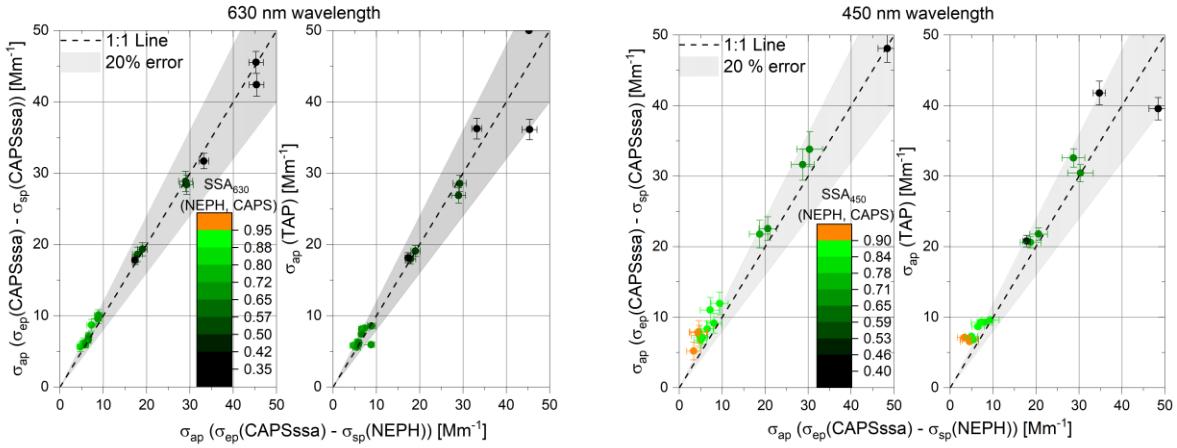
310

Figure 5. Scatter plots of measured 450 nm and 630 nm wavelength absorption coefficients of external mixtures of AQ and AS for different instrument combinations. The colour code represents the SSA value of the respective data point. An error band of ±20% was applied to the 1:1 line, which is required by Laj (2020) for light absorption measurements. Error bars shown represent propagated instrument precisions (1 σ).

315

In Figure 5, the light absorption measurements at wavelengths of 450 nm and 630 nm are compared. We chose to include 20% error bands for these comparisons, though the overall uncertainty for filter-based absorption measurements is often estimated to be 30% (Bond et al., 1999). Most of the data points shown fall within the 20% error band, with some exceptions for aerosols with low absorption and high SSA values.

320

Table 4. Linear regression results of scattering, σ_{sp} , extinction, σ_{ep}, and absorption, σ_{ap}, coefficients from Figures 3-5 for external mixtures of AQ and AS particles, given as slopes (m), Pearson R, and y-axis intercepts (b).

	$\sigma_{sp\,(CAPS)}$ vs. $\sigma_{sp\,(NEPH)}$	$\sigma_{sp(CAPS,TAP)}$ vs. $\sigma_{sp(NEPH)}$	$\sigma_{ep(NEPH,TAP)}$ vs. $\sigma_{ep(CAPS)}$	$\sigma_{ap(TAP)}$ vs. $\sigma_{ap(CAPS,NEPH)}$
			630 nm	
m	1.07 ± 0.03	1.08 ± 0.05	0.99 ± 0.03	0.92 ± 0.07

R	0.99	0.97	0.99	0.95
b [Mm^{-1}]	-1.84 ± 0.57	-2.15 ± 1.12	0.91 ± 0.93	0.78 ± 0.68
	450 nm			
m	0.99 ± 0.05	1.06 ± 0.03	0.98 ± 0.03	1.04 ± 0.08
R	0.97	0.99	0.99	0.96
b [Mm^{-1}]	1.14 ± 2.27	-4.60 ± 1.51	3.37 ± 1.71	2.13 ± 0.64

The high Pearson correlation (R > 0.95) coefficients in Table 4 indicate that the correlations are highly linear. The primary focus for this study was to have most of the experimental runs exhibit light extinctions between 5 Mm^{-1} and 150 Mm^{-1}, representative of atmospheric conditions. The slopes are all close to unity within the expected errors ranges, or at least single instrument uncertainty, indicating closure has been achieved for these optical measurements. Thus, the extensive parameters can be trusted for instrument comparison, especially for the light scattering and light extinction information. We provide regression analyses for all other absorbing aerosol types externally mixed with AS in Tables 7-9.

Excellent agreement (R>0.97) is shown for σ_{sp} measurements of the NEPH and the CAPS PM$_{SSA}$ scattering channel, indicating that the CAPS PM$_{SSA}$ scattering channel be considered as a substitute for the nephelometer scattering measurement. Trade-offs in the CAPS PM$_{SSA}$ versus NEPH comparison include the three wavelengths and backscatter measurements of the NEPH versus the single wavelength of the CAPS PM$_{SSA}$, countered by the additional extinction measurement of the CAPS PM$_{SSA}$ allowing for absorption and SSA values to be simultaneously measured.

In addition to regression analyses, where outliers and/or high values can dominate the fitted slope of the regression, another statistical approach is to investigate the ensemble averaged instrumental ratios (σ_{ap} (instrument #1) / σ_{ap} (instrument #2)), which is more sensitive to errors at low values. Resulting 630 nm and 450 nm wavelength absorption coefficient ratios are tabulated in Table 5 and 6, respectively. The average ratios are calculated from the points shown in Figure 5 for AQ and AS mixtures and from results obtained for the other absorbing particle types externally mixed with AS particles.

Table 5. Ensemble average ratios of σ_{ap} (TAP) / σ_{ap} (CAPS, NEPH) at 630 nm wavelength. N denotes the number of experiments used for the average.

630 nm wavelength	BC	AQ	SOOT	MB
σ_{ap} (TAP) / σ_{ap} (CAPS,NEPH)	1.22 ± 2.57 (N=36)	0.97 ± 0.22 (N=28)	1.10 ± 1.22 (N=25)	0.88 ± 0.17 (N=8)
σ_{ap} (TAP) / σ_{ap} (CAPS,NEPH) for samples with σ_{ap} >10 Mm^{-1}	1.08 ± 0.19 (N=24)	0.94 ± 0.10 (N=11)	0.86 ± 0.13 (N=6)	-

Table 5 demonstrates that the light absorption values agree for the different methods in general. With an ensemble average for the ratio σ_{ap} (TAP) / σ_{ap} (CAPS,NEPH) of 0.97 ± 0.22, good agreement is confirmed with over 60% of all

350   datapoints for external mixtures of AQ and AS falling within a range of σ_{ap} (TAP) / σ_{ap} (CAPS,NEPH) = {0.8 – 1.2}. These results support the linear regression results in Table 4, though exhibit larger scatter due to the greater sensitivity to small errors at low values.

The average ratios for other externally mixed absorbing aerosol types deviate more from unity than AQ mixtures.

355   Most of this scatter can be ascribed to the greater sensitivity of the ratio to small errors at low values. By filtering these ratios for points with $\sigma_{ap} > 10$ Mm^{-1}, approximately 80% of the data are within the range of 0.8-1.2, The ratios for $\sigma_{ap} < 10$ Mm^{-1} exhibited almost no modal value in the relative frequency distributions, confirming that scatter in low values significantly affects the average ratios.

360   **Table 6.** Ensemble average ratios of σ_{ap} (TAP) / σ_{ap} (CAPS, NEPH) at 450 nm wavelength. N denotes the number of experiments used for the average.

450 nm wavelength	BC	AQ	SOOT	MB
σ_{ap} (TAP) / σ_{ap} (CAPS,NEPH)	1.03 ± 1.72 (N=36)	1.06 ± 0.38 (N=28)	0.89 ± 1.05 (N=25)	1.28 ± 2.91 (N=8)
σ_{ap} (TAP) / σ_{ap} (CAPS,NEPH) for samples with σ_{ap} >10 Mm^{-1}	1.08 ± 0.33 (N=24)	1.01 ± 0.13 (N=11)	0.84 ± 0.27 (N=6)	-

Redoing this analysis for 450 nm wavelength, the light extinction and scattering of smaller particles increases compared to the values at 630 nm wavelength. As a result, the errors in calculating the 450 nm wavelength absorption

365   coefficients from the Differential Method also increase. As demonstrated in Table 6, only the variance for the ratio σ_{ap} (TAP) / σ_{ap} (CAPS, NEPH) for compact AQ particles was less than 1 (i.e., <100%), with over 50% of the data being within the range of 0.8-1.2. All ensemble average ratios were close to 1; however, with an associated error of up to ± 1.7 (i.e., $\pm 170\%$), these values are not significant, which means that the ratios scatter widely with no clear modal value. Again, filtering the 450 nm data for σ_{ap} >10 Mm^{-1} greatly improves the results, with ratios σ_{ap} (TAP) /

370   σ_{ap} (CAPS, NEPH) =1.08 ± 0.33 for BC. The best instrumental ratio of 1.01 ± 0.13 is shown for AQ mixtures in Table 6 at 450 nm wavelength.

375
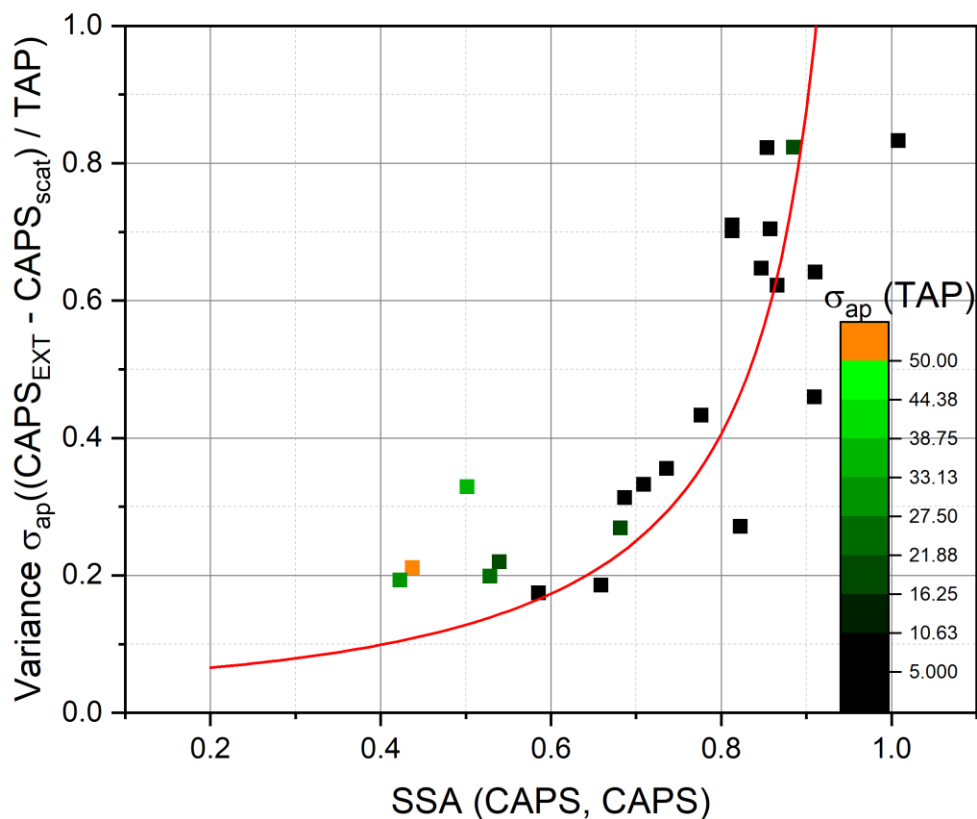
Figure 6. Variance of the measured absorption coefficients [σ_{ap} (CAPS, CAPS)) / σ_{ap} (TAP)] for Differential Method calculations relative to TAP measurements for AQ and AS external mixtures. The ratios are plotted against the aerosol measured SSA values [SSA(CAPS, CAPS)]. The red line represents the calculated relative errors using Gaussian error

380   propagation of the uncertainties of the DM Method with 1 as 100%..

In order to demonstrate the dependency of the uncertainties associated with the Differential Methods for deriving σ_{ap} values on the SSA, the ensemble variance ratios of σ_{ap} (CAPS, CAPS) / σ_{ap} (TAP) are shown as functions of SSA in Figure 6. For SSA values greater than 0.9, light absorption coefficients derived for the DM methods have propagated

385   uncertainties over 100% independently of their load.. The experimental data align within these calculated relative uncertainties.

Table 7. Linear regression results of scattering, σ_{sp}, extinction, σ_{ep}, and absorption, σ_{ap}, coefficients for external mixtures of BC and AS particles, given as slopes (m), Pearson R, and y-axis intercepts (b).

BC	$\sigma_{sp}(CAPS)$ vs $\sigma_{sp}(NEPH)$	$\sigma_{sp(CAPS,TAP)}$ vs. $\sigma_{sp(NEPH)}$	$\sigma_{ep(TAP,NEPH)}$ vs $\sigma_{ep(CAPS)}$	$\sigma_{ap(TAP)}$ vs. $\sigma_{ap(CAPS,NEPH)}$
		630 nm		
m	1.02 ± 0.03	0.99 ± 0.05	0.94 ± 0.02	0.90 ± 0.02
R	0.98	0.96	0.99	0.99
b [Mm^{-1}]	-0.69±0.7	-2.13 ± 1.01	3.59 ± 0.60	2.57 ± 0.11
		450 nm		
m	0.99 ± 0.02	1.06 ± 0.06	0.94 ± 0.03	0.86 ± 0.05
R	0.99	0.95	0.98	0.97
b [Mm^{-1}]	5.36 ± 1.45	-0.59 ± 3.86	0.97 ± 3.17	2.98 ± 0.48

390

Table 8. Linear regression results of scattering, σ_{sp}, extinction, σ_{ep}, and absorption, σ_{ap}, coefficients for external mixtures of SOOT and AS particles, given as slopes (m), Pearson R, and y-axis intercepts (b).

SOOT	$\sigma_{sp}(CAPS)$ vs $\sigma_{sp}(NEPH)$	$\sigma_{sp(CAPS,TAP)}$ vs. $\sigma_{sp(NEPH)}$	$\sigma_{ep(TAP,NEPH)}$ vs $\sigma_{ep(CAPS)}$	$\sigma_{ap(TAP)}$ vs. $\sigma_{ap(CAPS,NEPH)}$
		630 nm		
m	1.06 ± 0.04	0.9 ± 0.20	0.99 ± 0.08	0.76 ± 0.11
R	0.99	0.74	0.97	0.92
b [Mm^{-1}]	0.05 ± 0.56	1.57 ± 3.21	1.80 ± 1.72	3.93 ± 1.68
		450 nm		
m	0.81 ± 0.03	0.77 ± 0.07	0.92 ± 0.04	0.70 ± 0.10
R	0.99	0.97	0.98	0.91
b [Mm^{-1}]	1.73 ± 0.45	2.64 ± 0.91	3.26 ± 2.24	1.75 ± 0.82

Table 9. Linear regression results of scattering, σ_{sp}, extinction, σ_{ep}, and absorption, σ_{ap}, coefficients for external
395 mixtures of MB and AS particles, given as slopes (m), Pearson R, and y-axis intercepts (b).

MB	$\sigma_{sp}(CAPS)$ vs $\sigma_{sp}(NEPH)$	$\sigma_{sp(CAPS,TAP)}$ vs. $\sigma_{sp(NEPH)}$	$\sigma_{ep(TAP,NEPH)}$ vs $\sigma_{ep(CAPS)}$	$\sigma_{ap(TAP)}$ vs. $\sigma_{ap(CAPS,NEPH)}$
		630 nm		
m	0.96 ± 0.03	1.05 ± 0.03	0.96 ± 0.03	0.57 ± 0.10
R	0.99	0.99	0.99	0.94
b [Mm^{-1}]	0.42 ± 0.79	-0.95 ± 0.53	0.99 ± 0.51	1.06 ± 0.38
		450 nm		
m	1.02 ± 0.02	1.00 ± 0.16	0.89 ± 0.11	0.21 ± 0.14

Rb [Mm⁻¹]	0.99	0.95	0.97	0.58
	-1.85 ± 0.78	-0.82 ± 6.04	4.58 ± 4.88	3.43 ± 0.91

The linear regression analyses reporting fitted slopes, Pearson coefficients, and y-offsets for attenuation coefficients for external mixtures of AS and the different light absorbing aerosol types are presented in Table 7 (BC), Table 8 (SOOT), and Table 9 (MB). For 630 nm wavelength results, high Pearson coefficients (R>0.96) with negligible offsets (b<1 Mm⁻¹) and slopes ranging from 0.90 to 1.05 demonstrate good agreement (i.e., closure) for scattering and extinction coefficient measurements. Especially for MB and SOOT, the TAP measurements tend to overshoot the Differential method value by 20-40 %, whereas for BC the difference is only 10%. The reason could be that soot is a fractal agglomerate and in-situ methods as well as filter-based methods give different results as a function of the primary particle size (Sorensen et al., 2010) as well as of the previous mentioned filter-based artifacts, including changes of the slope at higher σ_{ap} (TAP) values. We measured values for BC ranging from 14 to 400 Mm⁻¹ for $\sigma_{ep,630nm}$, 1 to 322 Mm⁻¹ for $\sigma_{ap,630nm}$, and 12 to 174 Mm⁻¹ for $\sigma_{sp,630nm}$. For SOOT, we measured values ranging from 12 to 158 Mm⁻¹ for $\sigma_{ep,630nm}$, 1 to 322 Mm⁻¹ for $\sigma_{ap,630nm}$, and 5 to 80 Mm⁻¹ for $\sigma_{sp,630nm}$.

For 450 nm wavelength results, similar slopes, Pearson R, and y-offset values are reported. Linear regression slopes for SOOT decrease at the lower wavelength to a value of 0.77 for light scattering and 0.7 for light absorption. This decrease may well be an effect of the primary particles size of agglomeration, since those relationships change with the wavelength. For MB, the light absorption measurements using the DM method shows the highest difference compared to the TAP measurement with a regression slope of 0.21 ± 0.14. The reasons could include different absorption behaviour (i.e., filter-based artifacts) for filter-based method relative to in-situ measurements (Lack, 2008). Unfortunately, no clear understanding of the MB particle shape, phase, or uniformity could be made during this study.

3.3 Intensive Parameters of Aerosol Mixtures

3.2.1 Single scattering Albedo (SSA)

The Single Scattering Albedo (SSA), an important climate parameter, is investigated here as a relative measurement using multiple different methods of derivation to determine if closure between the different methods can be achieved. The SSA for different combinations of instruments are derived using Eq. (2) with the instruments used denoted in parentheses in Equations 7-10.

$$SSA(NEPH, TAP) = \frac{\sigma_{sp}(\text{NEPH})}{\sigma_{ap}(\text{TAP}) + \sigma_{sp}(\text{NEPH})} \qquad \text{Eq. (7)}$$

$$SSA(CAPS, TAP) = \frac{\sigma_{ep}(\text{CAPS}) - \sigma_{ap}(\text{TAP})}{\sigma_{ep}(\text{CAPS})} \qquad \text{Eq. (8)}$$

$$SSA(CAPS, CAPS) = \frac{\sigma_{sp}(\text{CAPS})}{\sigma_{ep}(\text{CAPS})} \qquad \text{Eq. (9)}$$

$$SSA(NEPH, CAPS) = \frac{\sigma_{sp}(\text{NEPH})}{\sigma_{ep}(\text{CAPS})} \qquad \text{Eq. (10)}$$

We have chosen to use the SSA(NEPH, CAPS) derived SSA values as a reference for these studies, as this method allows us to test the CAPS measured SSA with an independent, established method (Sheridan, 2005). However, a strong argument could be made that the CAPS PM_{SSA} Monitor derived SSA values should be the true reference here,
435   as the CAPS-derived SSA values were obtained by simultaneously measuring the scattering and extinction of same aerosol sample within a single instrument.
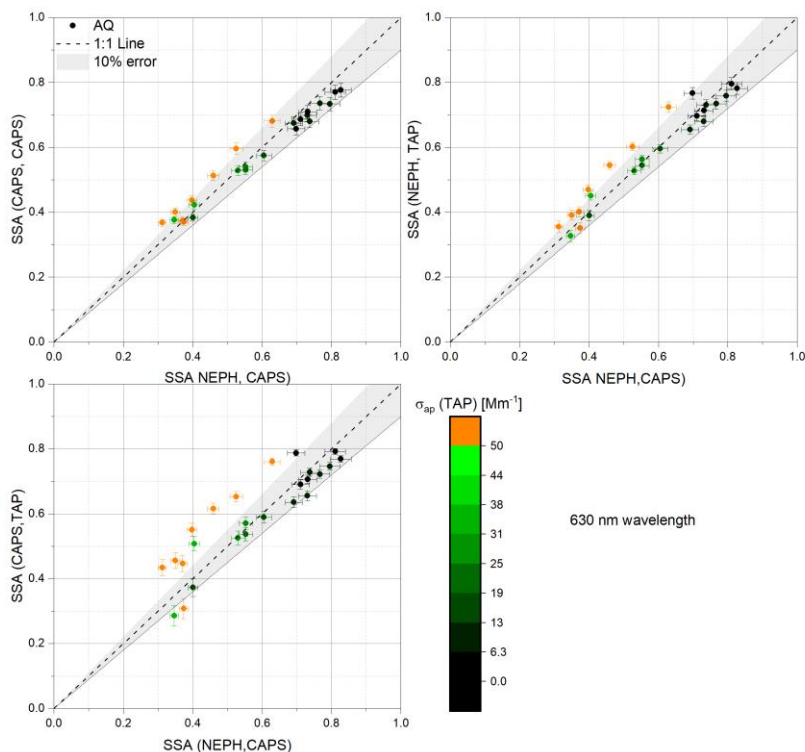
Figure 7. Scatter plots of derived SSA values from various combinations of measurements at 630 nm wavelength
440   obtained for AQ/AS mixtures (y-axis) versus SSA(NEPH, CAPS) as the reference on the x-axis. The colour code indicates σ_{ap}(TAP) values shown in Mm^{-1}.

Figure 7 shows the SSA values obtained by the three combinations of measurements at 630 nm wavelength. The correlations show reasonable results relative to a ±10% error band, with the best correlation obtained for the
445   SSA(CAPS, CAPS) versus SSA(NEPH, CAPS) measurements. In general, the higher the SSA values, the lower the measured absorption coefficients, σ_{ap}, reflecting that there are just fewer particles of Aquadag in the external aerosol mixture. The exception to this trend and the points exhibiting the greatest number of outliers (>10% from 1:1 line) are the points with high absorption coefficients (>50 Mm^{-1}). The largest outliers are observed in the instrument combinations that include the TAP and may be due to a nonlinear response in the TAP under high aerosol loadings.

450

Similar to the previous section, we calculated the ensemble instrument-to-instrument measurement ratio averages, using the SSA(NEPH, CAPS) values for reference, as another way of examining the correlations. The SSA values for all absorbing aerosol types (externally mixed with AS) are summarized in Table 10. The largest variance deviation is visible with combustion soot for TAP related data. The deviations of the reported mean from 1 are less than the relative uncertainties which range around 0.09.

455

Table 10. Ensemble instrument-to-instrument measurement ratio averages and standard deviations for different instrument combinations used to derive SSA values at 630 nm wavelength using $SSA(NEPH, CAPS)$ as reference.

Instrument combinations used for SSA calculations	BC	AQ	SOOT	MB
SSA (CAPS, CAPS) / SSA(NEPH, CAPS)	1.00 ± 0.08	1.01 ± 0.07	1.07 ± 0.07	1.00 ± 0.04
SSA(NEPH, TAP) / *SSA(NEPH, CAPS)*	0.96 ± 0.08	1.02 ± 0.08	1.04 ± 0.29	1.00 ± 0.03
SSA(CAPS, TAP) / SSA(NEPH, CAPS)	0.98 ± 0.16	1.05 ± 0.16	1.07 ± 0.51	1.00 ± 0.03

460
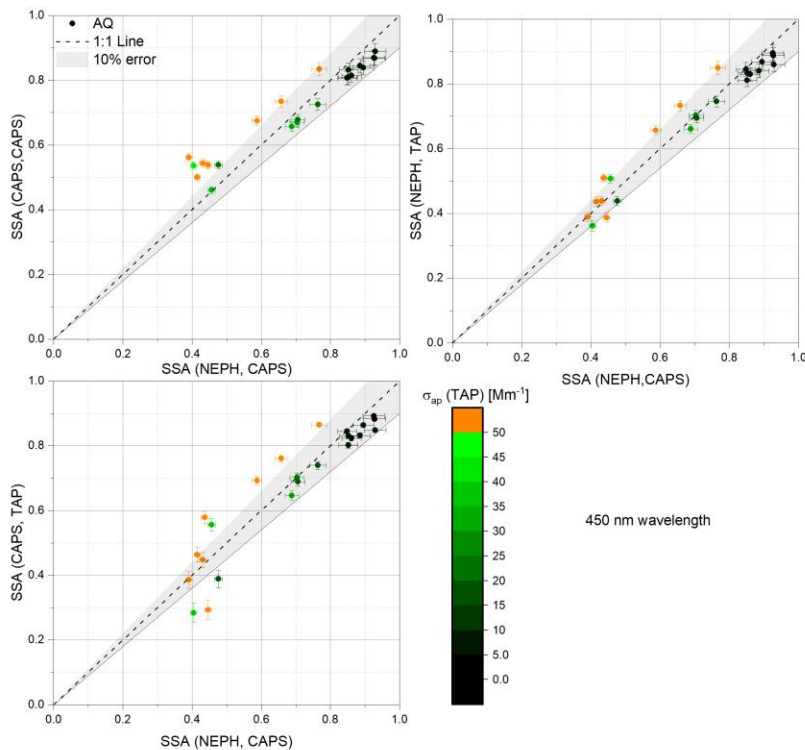
Figure 8. Scatter plots of Differential Method derived SSA values for different instrument combinations at 450 nm wavelength using AQ/AS mixtures versus SSA(NEPH, CAPS). The colour code indicates σ_{ap}(TAP) values shown in Mm^{-1}.

465

Figure **7**8 shows the SSA values obtained by the three combinations of measurements at 450 nm wavelength for all AQ/AS external mixtures. Observed patterns are comparable to the 630 nm wavelength results in Figure 7. For absorption coefficients up to 50 Mm^{-1}, all methods agree within 10%. Above 50 Mm^{-1}, the largest outliers are again observed in the instrument combinations that include the TAP instrument.

470

Table 11. Ensemble instrument-to-instrument measurement ratio averages and standard deviations for different instrument combinations used to derive SSA values at 450 nm wavelength using $SSA(NEPH, CAPS)$ as reference.

Instrument combination used for SSA calculation	BC	AQ	SOOT	MB
SSA (CAPS, CAPS) / $SSA(NEPH, CAPS)$	1.17 ± 0.21	1.04 ± 0.13	1.11 ± 0.13	0.98 ± 0.02
SSA (NEPH, TAP) / $SSA(NEPH, CAPS)$	1.07 ± 0.08	1.02 ± 0.08	0.96 ± 0.19	1.04 ± 0.13
SSA (CAPS, TAP) / $SSA(NEPH, CAPS)$	1.11 ± 0.13	1.03 ± 0.14	0.64 ± 0.38	1.05 ± 0.14

Table 11 summarizes the 450 nm wavelength ensemble instrument-to-instrument measurement ratio averages, using
475 the SSA(NEPH, CAPS) values for reference. The pattern that fractal aerosol optical properties appear to differ most from the reference values as the wavelength decreases is visible here, too. The fresh combustion soot aerosol shows the largest deviation from 1 (0.64 ± 0.38) for SSA (CAPS, TAP) measurements. But, overall, all the instrument-to-instrument ratios are unity within the observed variances.

480 *3.3.2 Ångström Exponents*
Ångström exponents are calculated from extensive parameters measured at different wavelengths. Even a small error in the extensive parameter measurements can result in a significant uncertainty in the derived Ångström exponents, considering error propagation. Some of optical instruments used in the current study operated at slightly different wavelengths, such that the derived Ångström exponents will exhibit slight biases due to these wavelength difference;
485 these biases are small relative to the observed variances and are thus assumed negligible.

The following equations, based on Eq.(3), are used to derive the Angström exponents for extinction, scattering, and absorption using different instrument combinations with their specific wavelengths indicated:

490
$$xAE(\text{Instrument1}, \text{Instrument 2}) = -\frac{\log\left(\frac{\sigma_{xp\lambda1}(\text{Instrument1},\text{Instrument 2})}{\sigma_{xp\lambda2}(\text{Instrument1},\text{Instrument 2})}\right)}{\log(\lambda1/\lambda2)}$$
Eq. (11)

$$EAE(\text{CAPS}) = -\frac{\log\left(\frac{\sigma_{ep\lambda1}(\text{CAPS})}{\sigma_{ep\lambda2}(\text{CAPS})}\right)}{\log(450/630)}$$
Eq. (12)

$$EAE(\text{NEPH}, \text{TAP}) = -\frac{\log\left(\frac{\sigma_{ep\lambda1}(\sigma_{ap}(\text{TAP})+\sigma_{sp}(\text{NEPH}))}{\sigma_{ep\lambda2}(\sigma_{ap}(\text{TAP})+\sigma_{sp}(\text{NEPH}))}\right)}{\log(450/630)}$$
Eq. (13)

$$SAE(\text{NEPH}) = -\frac{\log\left(\frac{\sigma_{sp\lambda1}(\text{NEPH})}{\sigma_{sp\lambda2}(\text{NEPH})}\right)}{\log(450/700)}$$
Eq. (14)

495
$$SAE(\text{CAPS}, \text{TAP}) = -\frac{\log\left(\frac{\sigma_{sp\lambda1}(\sigma_{ep}(\text{CAPS})-\sigma_{ap}(\text{TAP}))}{\sigma_{sp\lambda2}(\sigma_{ep}(\text{CAPS})-\sigma_{ap}(\text{TAP}))}\right)}{\log(450/630)}$$
Eq. (15)

$$AAE(\text{TAP}) = -\frac{\log\left(\frac{\sigma_{ap\lambda1}(\text{TAP})}{\sigma_{ap\lambda2}(\text{TAP})}\right)}{\log(467/652)}$$
Eq. (16)

$$AAE(\text{CAPS}, \text{NEPH}) = -\frac{\log\left(\frac{\sigma_{ap\lambda1}(\sigma_{ep}(\text{CAPS})-\sigma_{sp}(\text{NEPH}))}{\sigma_{ap\lambda2}(\sigma_{ep}(\text{CAPS})-\sigma_{sp}(\text{NEPH}))}\right)}{\log(450/630)}$$
Eq. (17)

3.2.3 Extinction Ångström Exponents (EAE)

500 The derived EAE(NEPH, TAP) and EAE(CAPS) values are shown in Figure 9 as a scatter plot and in Figure 10 as a ratio versus the 630 nm wavelength SSA(NEPH, CAPS) values. The EAE(CAPS) values were used as the reference measurement. When directly comparing EAE(NEPH, TAP) to EAE(CAPS), the EAE values agree within 10% variance. The highest measured EAE values for the AQ and AS mixtures, ~3, were close to the EAE values measured for the pure AS particles distributions with CMD ~ 40 nm (Table 3). The measured EAE(NEPH, TAP) / EAE(CAPS)

505 ratios exhibited no systematic dependence on the σ_{ap}(TAP), Figure 9, or SSA(NEPH, CAPS), Figure 10, values. Measured EAE(NEPH, TAP) / EAE(CAPS) ratios for all absorbing aerosol types (externally mixed with AS) are listed in Table 12.
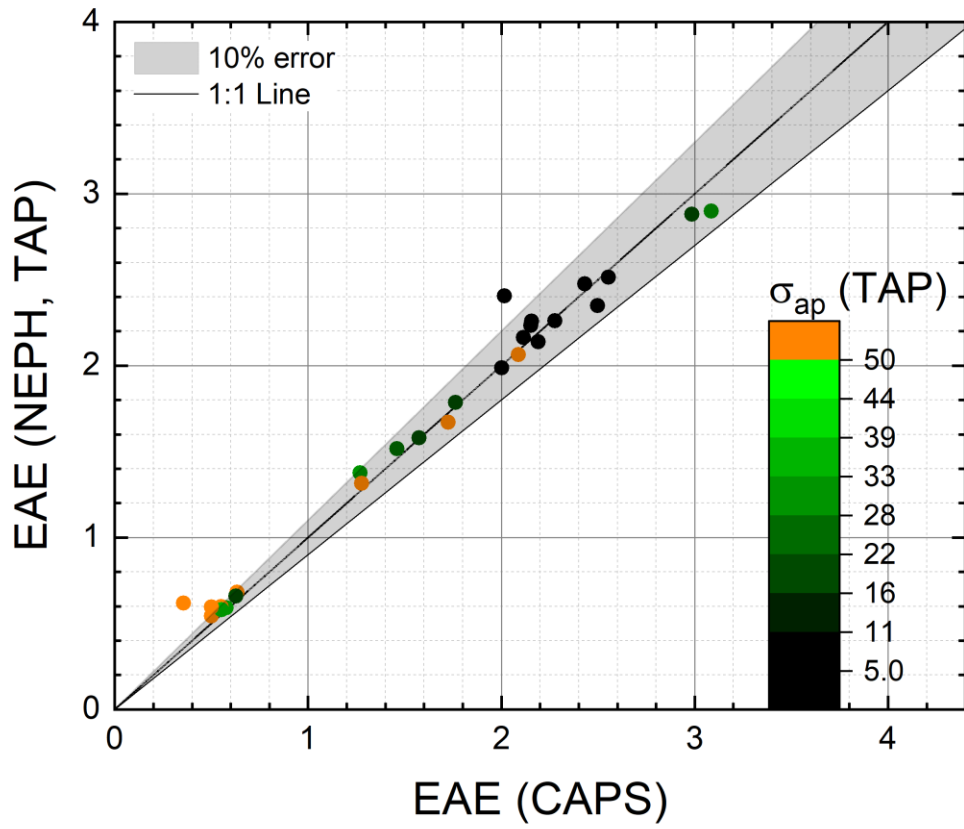
Figure 9. Scatter plot of EAE(NEPH, TAP) measurements compared to EAE(CAPS) measurements for AQ/AS mixtures. An error band of 10% is shown.
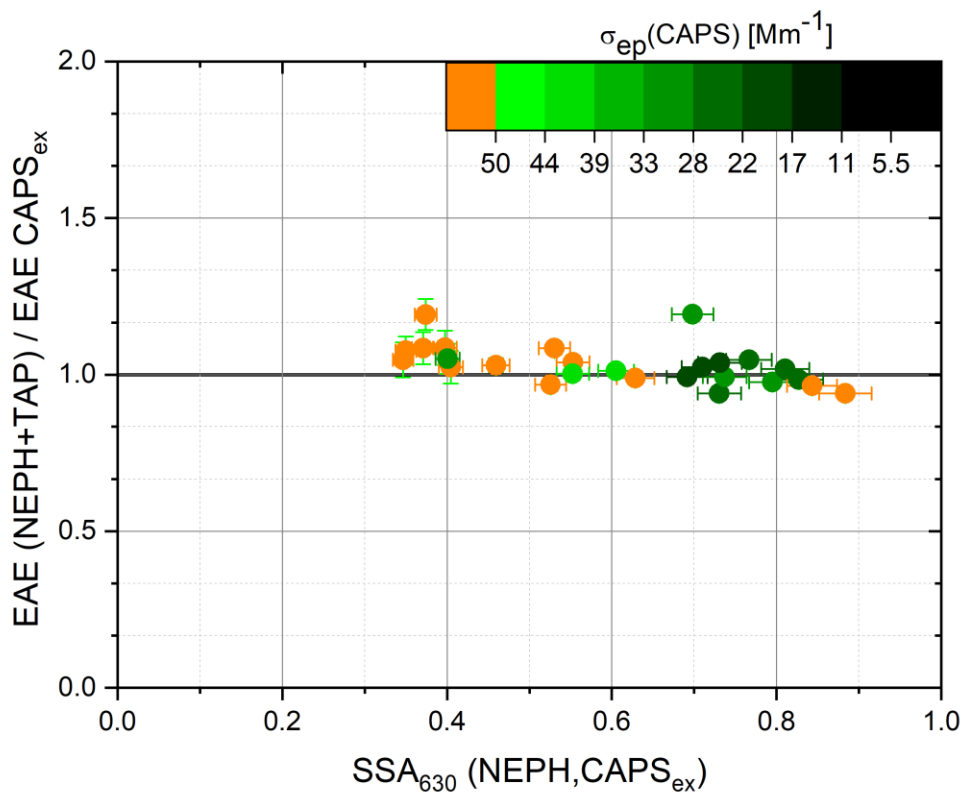
Figure 10. The extinction Ångström exponent EAE(NEPH, TAP) / EAE(CAPS) ratios as a function of 630nm wavelength SSA(NEPH, CAPS) values for AQ/AS mixtures. The 630 nm wavelength light absorption coefficient, σ_{ep}(CAPS), is used as the colour code.

3.3.4 Scattering Ångström exponent (SAE)

The derived SAE(CAPS, TAP) and SAE(NEPH) values are shown in Figure 11 as a scatter plot and in Figure 12 as a ratio versus the 630 nm wavelength SSA(NEPH, CAPS) values. The SAE(NEPH) values were used as the reference measurement. All SAE(CAPS, TAP) and SAE(NEPH) values agree within 10% variance and the measured SAE(CAPS, TAP) / SAE(NEPH) ratios exhibited no systematic dependence on the σ_{sp}(CAPS) for 630 nm wavelength, Figure 11, or SSA(NEPH, CAPS), Figure 12, values. The measured SAE(CAPS, TAP) / SAE(NEPH) ratios for all absorbing aerosol types (externally mixed with AS) are listed in Table 12.
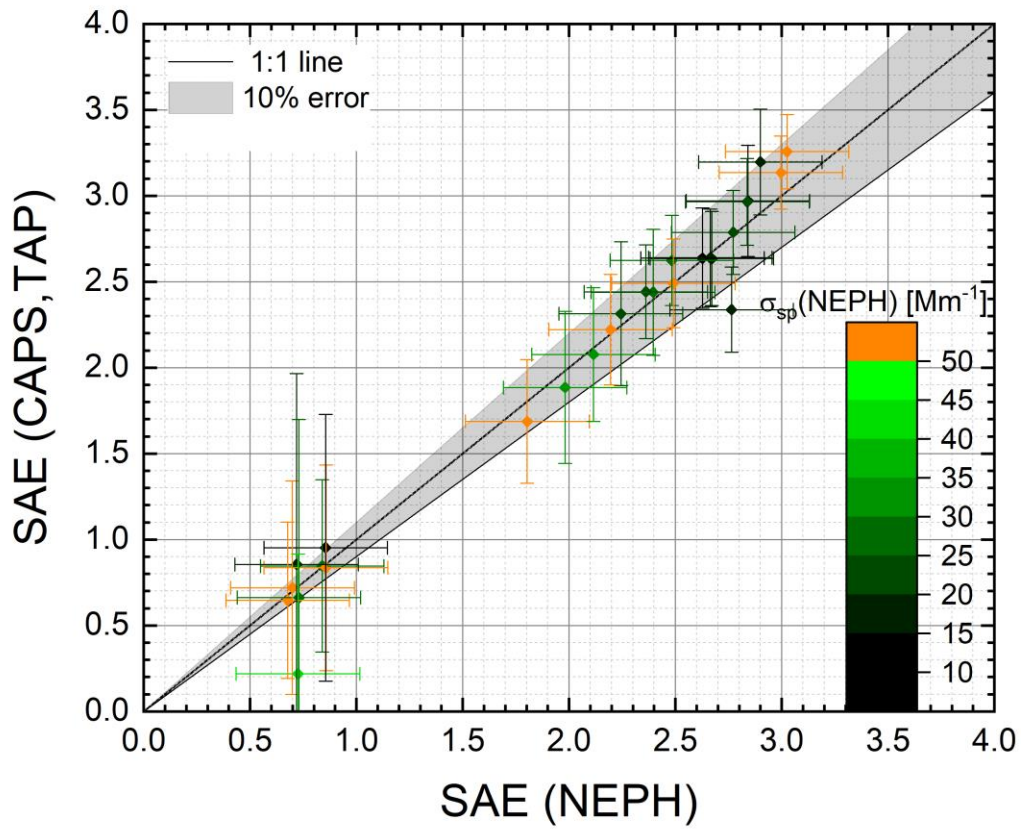
525

Figure 91. Scatter plot of SAE(CAPS,TAP) measurements compared to SAE(NEPH) measurements for AQ/AS mixtures. An error band of 10% is shown.
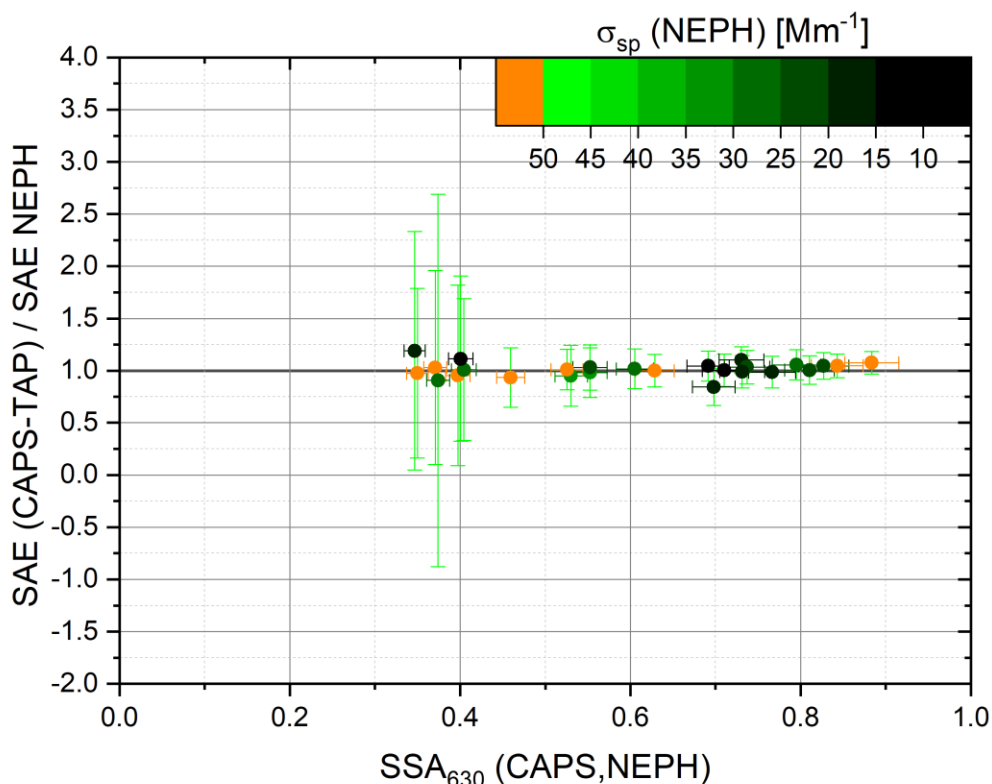
Figure 102. The scattering Ångström exponent ratio, SAE(CAPS, TAP) / SAE(NEPH), as a function of 630nm
wavelength SSA(NEPH, CAPS) values for AQ/AS mixtures. The 630 nm wavelength light absorption coefficient,
σ_{ap}(TAP), is used as the colour code.

3.3.5 Absorbing Ångström exponent (AAE)

The absorption Ångström exponent (AAE) depends entirely on the absorbing particle type and coatings and should
not differ when the light absorbing particles are externally mixed with non-light absorbing particles. Thus, scatter
plots of AAE values should exhibit a single point. Figure 13 shows the derived AAE(CAPS, NEPH) values relative
to the derived AAE(TAP) values for pure AQ and for AQ/AS external mixtures. The AAE(TAP) values were chosen
as the reference measurements here, despite the potential for known filter-based artifacts. The pure AQ measurements
in Figure 13 exhibit a compact cluster around AAE ~ 0.4, indicating a well-defined (i.e., small variance) set of AAE
measurements were obtained for both AAE measurements. The measured AAE for pure AQ particles of 0.4 is
consistent with the "close to zero" result reported byAiken. (2016).

The externally mixed AQ/AS results show a significantly different result. For the AQ/AS mixtures, the AAE(TAP)
exhibited a similar variance as for the pure AQ aerosols, while the AAE(CAPS, NEPH) values exhibited a much larger
variance, including unphysical negative values. One reason for the larger AAE(CAPS, NEPH) variances observed for
the externally AQ/AS mixtures relative to the pure AQ is that the mixed AQ/AQ samples were conducted at

significantly lower AQ loadings (i.e., lower σ_{ap} values). Another reason is that the pure AQ aerosols exhibited the lowest SSA values (~0.37 from Table 3) relative to the AQ/AS external mixtures.

550   Figure 14 shows the ratio AAE(CAPS, NEPH) / AAE(TAP) versus the 630 nm wavelength SSA(NEPH, CAPS) values. As predicted in the propagated error analysis shown in Figure 6, higher SSA values cause higher uncertainties in Differential Method calculated light absorption coefficients, σ_{ap}(DM), and, therefore, the derived AAE(CAPS, NEPH) values. In fact, since the derived AAE(CAPS, NEPH) values depend upon σ_{ap}(DM) measurements at two different wavelengths, the AAE uncertainties will be significantly higher than the corresponding σ_{ap}(DM)

555   uncertainties, especially at high SSA values. Figure 14 indicates that lowering the absorption coefficients below 50 Mm^{-1} or increasing the SSA above 0.5, the derived AAE(CAPS, NEPH) values begin to vary strongly relative to the AAE(TAP) values. For laboratory studies, aerosols with similar low SSA values and high absorbing particle concentrations can be readily achieved, but are rarely present in the ambient atmosphere. Therefore, extreme caution is justified when attempting to derive AAE(CAPS, NEPH) values for atmospheric measurements.

560
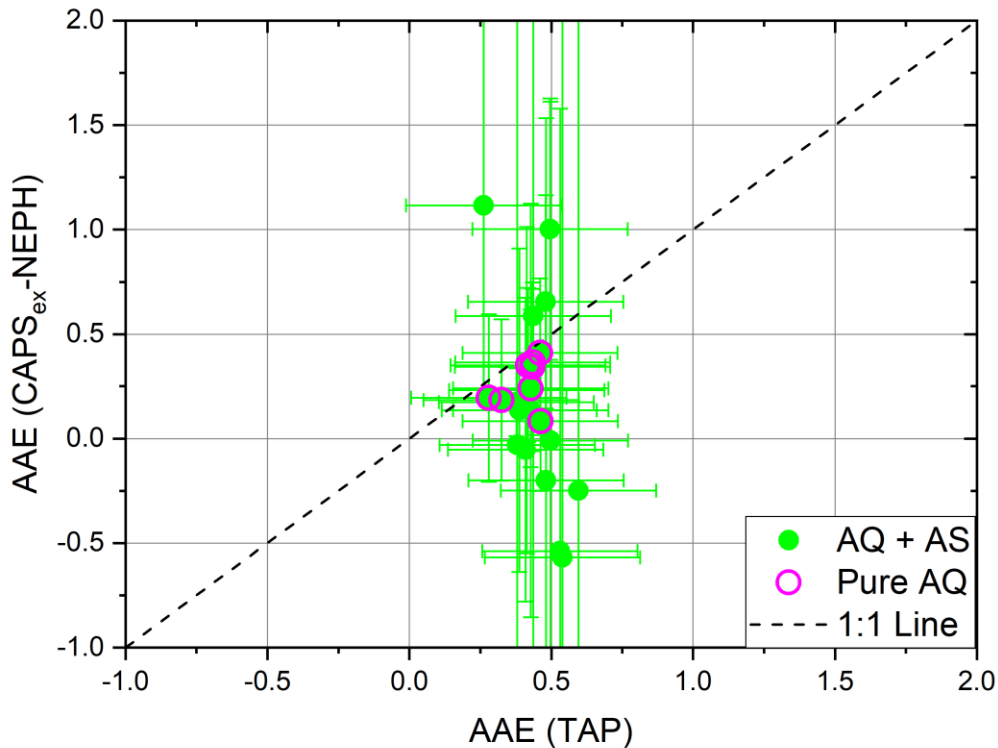
Figure 11. Scatter plot of AAE(CAPS, NEPH) measurements compared to AAE(TAP) measurements for pure AQ and AQ/AS external mixtures. Measured precision error bars are shown for individual AQ/AS externally mixed measurements.
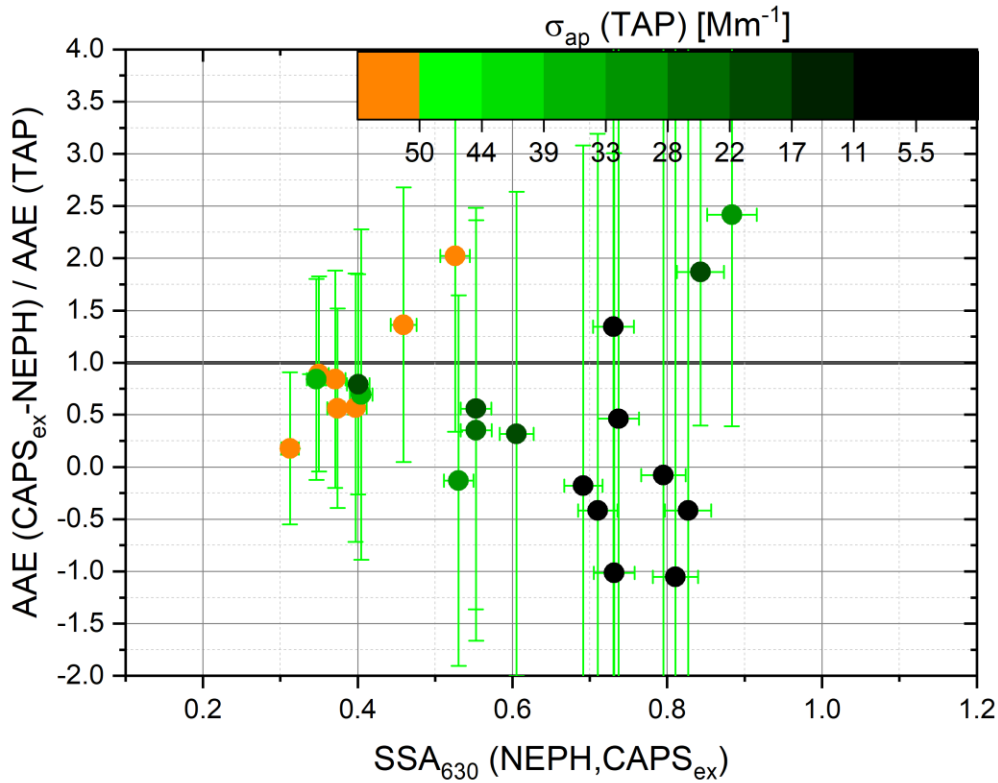
Figure 12. The absorbing Ångström exponent ratio, AAE(CAPS, NEPH) / AAE(TAP), as a function of 630 nm wavelength SSA(NEPH, CAPS) values for AQ/AS mixtures. The 630 nm wavelength light absorption coefficient, σ_{ap}(TAP), is used as the colour code. Measured precision error bars are shown for individual measurements.

Table 12 summarizes the averages and standard deviations of the measured Ångström exponent ratios, EAE(NEPH, TAP) / EAE(CAPS), SAE(CAPS, TAP) / SAE(NEPH), and AAE(CAPS, NEPH) / AAE(TAP). The average Ångström exponent ratios for light extinction (EAE) and scattering (SAE) fall within 10% of unity, with SOOT exhibiting the large variances. The average Ångström exponent ratios for light absorption (AAE) exhibit large deviations from unity

 with even larger variances. A large deviation for the AAE ratios value is associated with weak absorption coefficients of the aerosol mixtures used. Therefore, the AAE values show the biggest differences within the instrument-to-instrument ratio analysis.

Table 12. Ensemble averages and standard deviations for the instrument-to-instrument ratios of the Ångström
 exponents (EAE, SAE, AAE) derived from multiple instruments relative to those derived from single instruments as reference.

Ångström coefficient ratio	BC	AQ	SOOT	MB

EAE(NEPH, TAP) / EAE(CAPS)	0.92 ± 0.07	1.05 ± 0.15	0.99 ± 0.56	0.97 ± 0.15
SAE(CAPS, TAP) / SAE(NEPH)	1.13 ± 0.10	0.99 ± 0.15	1.43 ± 0.61	1.09 ± 0.15
AAE(CAPS, NEPH) / AAE(TAP)	1.72 ± 0.85	0.39 ± 1.70	1.19 ± 0.93	0.91 ± 2.32

4. Conclusions

585

A major goal of this study was to determine if the intensive optical aerosol parameters, single scattering albedo and Ångström exponents, for externally mixed absorbing and non-absorbing aerosols could be measured within reported optical instrument extensive measurement uncertainties (i.e., optical closure). Closure within reported instrument uncertainties was achieved for all measured extensive optical properties (i.e., extinction, scattering, and absorption)

590 and most intensive optical properties (i.e., single scattering albedo, extinction Ångström exponent and scattering Ångström exponent). Unsurprisingly, the measurements with the largest variances were the absorption coefficient measurements derived from the Differential Method (i.e., absorption = extinction minus scattering) and the related absorbing Ångström exponent (AAE). While the absorption coefficient measurements were within reported uncertainties, the derived AAE values exhibited average values and standard deviations far greater than the other

595 Ångström exponent but are within expected range.

We conducted an instrument intercomparison laboratory study employing several widely used measurement techniques suitable for long-term ambient observations. The optical instrument suite included two CAPS PM$_{SSA}$ monitors measuring extinction and scattering at 450 and 630nm, a TSI integrating Nephelometer (NEPH) measuring

600 scattering at 450, 550, and 700 nm, and a Brechtel Tricolor Absorption Photometer (TAP) measuring absorption at 467, 528, and 652 nm. External mixtures of absorbing (Aquadag, combustion soot from a laboratory flame generator, Cabot carbon black, and acrylic Magic Black paint) particles and non-absorbing ammonium sulphate particles were generated with single scattering albedo (SSA) values between 0.2 and 1.0 and extinction values between 15 – 150 Mm^{-1}, representative of atmospheric aerosols. However, our study does not explicitly address real-world ambient

605 aerosols that can be internally or externally mixed or both, contain particles with liquid, solid, and/or semi-solid phases, and may contain multiple sources of absorbing material.

Overall, we were able to show that measured extensive optical parameters agree within the limits of uncertainty for the individual or combined instruments. In particular, we report that the scattering coefficient measurement by the

610 CAPS PM$_{SSA}$ agrees with the TSI integrating Nephelometer within 10% relative error (i.e., optical closure). Therefore, The CAPS PM$_{SSA}$ monitor could be considered as a replacement for the TSI Nephelometer, as the NEPH is no longer produced. Trade-offs in the CAPS PM$_{SSA}$ versus NEPH comparison include the three wavelengths and backscatter measurements of the NEPH versus the single wavelength of the CAPS PM$_{SSA}$, countered by the additional extinction measurement of the CAPS PM$_{SSA}$ allowing for absorption and SSA values to be simultaneously measured.

615

Measurement differences were observed as a function of absorbing particle type. For light absorbing compact aggregates, we achieved the highest correlations for light extinction, scattering, and absorption coefficients. For fractal-like absorbing combustion soot particles, the correlation for light absorption between the in-situ and filter
620 methods weakened but stayed within instrument uncertainty ranges. These observed differences might be due to the combined effects of small flickers from the inverted flame generator during the experiment, the overall filter correction schemes, and/or the physical behaviour of agglomerates. For more compact particles, the scattering is stronger (Radney et al., 2014). For the TAP filtered-based method, changes in the backscattering of light is not considered in the correction schemes, which might be responsible for the disagreement.

625

Uncertainties increased for intensive optical parameters, especially for the absorption Ångström exponent (AAE) parameter that relied on the differential method to calculate light absorption as the difference between light extinction and light scattering. The intensive parameters for the scattering and extinction Ångström exponent were within 10% relative error (i.e., optical closure), regardless of which instrument combination was used for parameter derivation. In
630 contrast, absorption Ångström exponent (AAE) values required low SSA values (<0.5) and high particulate absorption values (>50 Mm^{-1}) were necessary to reach satisfactory levels of measurement uncertainty. Similar AAE results were recently reported for rural background sampling (Asmi et al., 2021).

Finally, Laj et al. (2020) recently stated measurement requirements for GCOS (Global Climate Observing System)
635 applications for attributing and detecting changes to climate feedback. The reported requirements for the climate-critical intensive optical properties, specifically the single scattering albedo (SSA), are measurement techniques with relative measurement uncertainties less than 20%. In our study, SSA values were measured for all instrument combinations of CAPS, TAP, and NEPH within 10% relative error at 630 nm wavelength and within 15% at 450 nm wavelength. Therefore, the measured SSA averages and variances using our optical instrument suite for externally
640 mixed laboratory particles indicates that these instruments meet these proposed requirements.

Acknowledgments. Parts of this work were supported by IAGOS-D (Grant Agreement No. 01LK1301A), EU H2020 Project ENVRIplus (Grant No.654182) and HITEC Graduate School for Energy and Climate. A special thanks to Paola Formenti for her assistance with the manuscript.

645

Contributions of co-authors. PW performed all instrument calibrations, the instrumental set up, and the data analysis. UB and BF designed the LabVIEW environment of the experimental set up. MB helped during instrument preparations. AF and TO provided technical details of the instrumentation. PW, OB,, AF, TO, UB and AP contributed to the manuscript and the interpretation of the results.

650

Conflict of interest. The authors declare that they have no conflict of interest.

References

Anderson, T. L. and Ogren, J. A.: Determining aerosol radiative properties using the TSI 3563 integrating
655   nephelometer, Aerosol Science and Technology, 29, 57-69, 1998.

Ångström, A.: On the Atmospheric Transmission of Sun Radiation and on Dust in the Air, Geografiska Annaler, 11, 156-166, 1929.

Barber, P. W. and Wang, D.-S.: Rayleigh-Gans-Debye applicability to scattering by nonspherical particles, Appl. Opt., 17, 797-803, 1978.

660 Bischof, O., Weber, P., Bundke, U., Petzold, A., and Kiendler-Scharr, A.: Characterization of the Miniaturized Inverted Flame Burner as a Combustion Source to Generate a Nanoparticle Calibration Aerosol, doi: 10.1007/s40825-019-00147-, 2019. 1-10, 2019.

Bodhaine, B. A., Ahlquist, N. C., and Schnell, R. C.: Three-wavelength nephelometer suitable for aircraft measurement of background aerosol scattering coefficient, Atmospheric Environment. Part A. General
665   Topics, 25, 2267-2276, 1991.

Bohren, C. F. and Huffman, D. R.: Absorption and scattering of light by small particles, 1983.

Bond, T. C., Anderson, T. L., and Campbell, D.: Calibration and intercomparison of filter-based measurements of visible light absorption by aerosols, Aerosol Science and Technology, 30, 582-600, 1999.

Collaud Coen, M., Weingartner, E., Apituley, A., Ceburnis, D., Fierz-Schmidhauser, R., Flentje, H., Henzing, J. S.,
670   Jennings, S. G., Moerman, M., Petzold, A., Schmid, O., and Baltensperger, U.: Minimizing light absorption measurement artifacts of the Aethalometer: evaluation of five correction algorithms, Atmos. Meas. Tech., 3, 457-474, 2010.

Faria, J., Bundke, U., Freedman, A., Onasch, T., and Petzold, A.: Laboratory Validation and Field Deployment of a Compact Single-Scattering Albedo (SSA) Monitor, Atmospheric Measurement Techniques Discussions, doi:
675   10.5194/amt-2019-146, 2019. 1-18, 2019.

Formenti, P., Schütz, L., Balkanski, Y., Desboeufs, K., Ebert, M., Kandler, K., Petzold, A., Scheuvens, D., Weinbruch, S., and Zhang, D.: Recent progress in understanding physical and chemical properties of African and Asian mineral dust, Atmos. Chem. Phys., 11, 8231-8256, 2011.

Foster, K., Pokhrel, R., Burkhart, M., and Murphy, S.: A novel approach to calibrating a photoacoustic absorption
680   spectrometer using polydisperse absorbing aerosol, Atmos. Meas. Tech., 12, 3351-3363, 2019.

Hansen, A. D. A., Rosen, H., and Novakov, T.: The aethalometer — An instrument for the real-time measurement of optical absorption by aerosol particles, Science of The Total Environment, 36, 191-196, 1984.

Kaskaoutis, D. G., Kambezidis, H. D., Hatzianastassiou, N., Kosmopoulos, P. G., and Badarinath, K. V. S.: Aerosol climatology: on the discrimination of aerosol types over four AERONET sites, Atmos. Chem. Phys. Discuss.,
685   2007, 6357-6411, 2007.

Kazemimanesh, M., Moallemi, A., Thomson, K., Smallwood, G., Lobo, P., and Olfert, J.: A novel miniature inverted-flame burner for the generation of soot nanoparticles, Aerosol Science and Technology, doi: 10.1080/02786826.2018.1556774, 2018. 2018.

Kim, J., Bauer, H., Dobovičnik, T., Hitzenberger, R., Lottin, D., Ferry, D., and Petzold, A.: Assessing Optical
690   Properties and Refractive Index of Combustion Aerosol Particles Through Combined Experimental and Modeling Studies, Aerosol Science and Technology, 49, 340-350, 2015.

Kirchstetter, T. W. and Thatcher, T. L.: Contribution of organic carbon to wood smoke particulate matter absorption of solar radiation, Atmos. Chem. Phys., 12, 6067-6072, 2012.

Kokhanovsky, A.: Aerosol Optics: Light Absorption and Scattering by Particles in the Atmosphere, 2008.

695 Massoli, P., Murphy, D. M., Lack, D. A., Baynard, T., Brock, C. A., and Lovejoy, E. R.: Uncertainty in Light Scattering Measurements by TSI Nephelometer: Results from Laboratory Studies and Implications for Ambient Measurements, Aerosol Science and Technology, 42, 1064-1074, 2009.

Modini, R. L., Corbin, J. C., Brem, B. T., Irwin, M., Bertò, M., Pileci, R. E., Fetfatzis, P., Eleftheriadis, K., Henzing, B., Moerman, M. M., Liu, F., Müller, T., and Gysel-Beer, M.: Detailed characterization of the CAPS single-scattering albedo monitor (CAPS PMssa) as a field-deployable instrument for measuring aerosol light absorption with the extinction-minus-scattering method, Atmos. Meas. Tech., 14, 819-851, 2021.

Moosmüller, H., Chakrabarty, R. K., and Arnott, W. P.: Aerosol light absorption and its measurement: A review, Journal of Quantitative Spectroscopy and Radiative Transfer, 110, 844-878, 2009.

Müller, T., Virkkula, A., and Ogren, J. A.: Constrained two-stream algorithm for calculating aerosol light absorption coefficient from the Particle Soot Absorption Photometer, Atmos. Meas. Tech., 7, 4049-4070, 2014.

Myhre, G., Shindell, D., Bréon, F.-M., Collins, W., Fuglestvedt, J., Huang, J., Koch, D., Lamarque, J.-F., Lee, D., Mendoza, B., Nakajima, T., Robock, A., Stephens, G., Takemura, T., and Zhang, H.: Anthropogenic and Natural Radiative Forcing. In: Climate Change 2013: The Physical Science Basis. Contribution of Working Group I to the Fifth Assessment Report of the Intergovernmental Panel on Climate Change, Stocker, T. F., Qin, D., Plattner, G.-K., Tignor, M., Allen, S. K., Boschung, J., Nauels, A., Xia, Y., Bex, V., and Midgley, P. M. (Eds.), Cambridge University Press, Cambridge, United Kingdom and New York, NY, USA, 2013.

Ogren, J., Wendell, J., Andrews, E., and Sheridan, P.: Continuous light absorption photometer for long-Term studies, Atmospheric Measurement Techniques, 10, 4805-4818, 2017.

Onasch, T., Massoli, P., Kebabian, P., Hills, F. B., Bacon, F., and Freedman, A.: Single Scattering Albedo Monitor for Airborne Particulates, Aerosol Science and Technology, 49, 267 - 279, 2015.

Petzold, A., Ogren, J. A., Fiebig, M., Laj, P., Li, S. M., Baltensperger, U., Holzer-Popp, T., Kinne, S., Pappalardo, G., Sugimoto, N., Wehrli, C., Wiedensohler, A., and Zhang, X. Y.: Recommendations for reporting "black carbon" measurements, Atmos. Chem. Phys., 13, 8365-8379, 2013.

Petzold, A., Rasp, K., Weinzierl, B., Esselborn, M., Hamburger, T., DöRnbrack, A., Kandler, K., SchuüTz, L., Knippertz, P., Fiebig, M., and Virkkula, A.: Saharan dust absorption and refractive index from aircraft-based observations during SAMUM 2006, Tellus B: Chemical and Physical Meteorology, 61, 118-130, 2009.

Petzold, A., Schloesser, H., Sheridan, P., Arnott, W., Ogren, J., and Virkkula, A.: Evaluation of Multiangle Absorption Photometry for Measuring Aerosol Light Absorption, Aerosol Science and Technology, 39, 40-51, 2005.

Rosen, H., Hansen, A. D. A., Gundel, L., and Novakov, T.: Identification of the optically absorbing component in urban aerosols, Appl. Opt., 17, 3859-3861, 1978.

Russell, P. B., Bergstrom, R. W., Shinozuka, Y., Clarke, A. D., DeCarlo, P. F., Jimenez, J. L., Livingston, J. M., Redemann, J., Dubovik, O., and Strawa, A.: Absorption Angstrom Exponent in AERONET and related data as an indicator of aerosol composition, Atmos. Chem. Phys., 10, 1155-1169, 2010.

Sandradewi, J., Prévôt, A. S. H., Szidat, S., Perron, N., Alfarra, M. R., Lanz, V. A., Weingartner, E., and Baltensperger, U.: Using Aerosol Light Absorption Measurements for the Quantitative Determination of Wood Burning and Traffic Emission Contributions to Particulate Matter, Environmental Science & Technology, 42, 3316-3323, 2008.

Schnaiter, M., Schmid, O., Petzold, A., Fritzsche, L., Klein, K. F., Andreae, M. O., Helas, G., Thielmann, A., Gimmler, M., Mohler, O., Linke, C., and Schurath, U.: Measurement of wavelength-resolved light absorption by aerosols utilizing a UV-VIS extinction cell, Aerosol Science and Technology, 39, 249-260, 2005.

Sheridan, P. J., Arnott, W. P., Ogren, J. A., Andrews, E., Atkinson, D. B., Covert, D. S., Moosmüller, H., Petzold, A., Schmid, B., Strawa, A. W., Varma, R., and Virkkula, A.: The Reno Aerosol Optics Study: An Evaluation of Aerosol Absorption Measurement Methods, Aerosol Science and Technology, 39, 1-16, 2005.

Veselovskii, I., Goloub, P., Podvin, T., Bovchaliuk, V., Derimian, Y., Augustin, P., Fourmentin, M., Tanre, D., Korenskiy, M., Whiteman, D. N., Diallo, A., Ndiaye, T., Kolgotin, A., and Dubovik, O.: Retrieval of optical and physical properties of African dust from multiwavelength Raman lidar measurements during the SHADOW campaign in Senegal, Atmos. Chem. Phys., 16, 7013-7028, 2016.

Virkkula, A.: Correction of the Calibration of the 3-wavelength Particle Soot Absorption Photometer (3 PSAP), Aerosol Science and Technology, 44, 706-712, 2010.

Xu, L., Suresh, S., Guo, H., Weber, R. J., and Ng, N. L.: Aerosol characterization over the southeastern United States using high-resolution aerosol mass spectrometry: spatial and seasonal variation of aerosol composition and sources with a focus on organic nitrates, Atmos. Chem. Phys., 15, 7307-7336, 2015.